

Tuning the electronic and the crystalline structure of LaBi by pressure

F. F. Tafti,^{1,2,*} M. S. Torikachvili,³ R. L. Stillwell,⁴ B. Baer,⁴ E. Stavrou,⁴ S. T. Weir,⁴ Y. K. Vohra,⁵
H.-Y. Yang,¹ E. F. McDonnell,¹ S. K. Kushwaha,² Q. D. Gibson,² R. J. Cava,² and J. R. Jeffries⁴

¹*Department of Physics, Boston College, Boston, MA, USA*

²*Department of Chemistry, Princeton University, NJ, USA*

³*Department of Physics, San Diego State University, San Diego, CA, USA*

⁴*Lawrence Livermore National Laboratory, Livermore, CA, USA*

⁵*Department of Physics, University of Alabama at Birmingham, Birmingham, AB, USA*

(Dated: November 17, 2021)

Extreme magnetoresistance (XMR) in topological semimetals is a recent discovery which attracts attention due to its robust appearance in a growing number of materials. To search for a relation between XMR and superconductivity, we study the effect of pressure on LaBi taking advantage of its simple structure and simple composition. By increasing pressure we observe the disappearance of XMR followed by the appearance of superconductivity at $P \approx 3.5$ GPa. The suppression of XMR is correlated with increasing zero-field resistance instead of decreasing in-field resistance. At higher pressures, $P \approx 11$ GPa, we find a structural transition from the face center cubic lattice to a primitive tetragonal lattice in agreement with theoretical predictions. We discuss the relationship between extreme magnetoresistance, superconductivity, and structural transition in LaBi.

PACS numbers: 73.43.Qt, 64.70.K-, 74.62.Fj, 71.20.Lp

I. INTRODUCTION

Extreme magnetoresistance is an enormous increase of electrical resistance in response to a modest magnetic field in several topological semimetals including Cd_3As_2 , Na_3Bi , NbAs , NbP , TaAs , NbSb_2 , TaSb_2 , WTe_2 , $(\text{Zr}/\text{Hf})\text{Te}_5$.^{1–10} Recent studies on $(\text{W}/\text{Mo})\text{Te}_2$ and $(\text{Zr}/\text{Hf})\text{Te}_5$ suggest that pressure suppresses the extreme magnetoresistance (XMR) and gives rise to superconductivity.^{11–14} Common to all these materials is a rapid onset of superconductivity at the pressure where XMR is suppressed, followed by a slow suppression of T_c with further increasing pressure. For example, MoTe_2 is superconducting at zero pressure with $T_c = 0.1$ K which rapidly increases to 8 K by applying only 1 GPa of pressure.¹⁵ WTe_2 is not superconducting at $P = 0$, it shows an incomplete superconducting transition at $P = 2.5$ GPa and a full transition at $P = 8$ GPa.^{11,12} Similarly, ZrTe_5 is not superconducting at $P = 0$, it shows a sudden onset of superconductivity at $P = 6.7$ GPa with a subsequent T_c discontinuity at $P = 20$ GPa attributed to a second superconducting state.¹³ By pressurizing LaBi we reveal all the above-mentioned characteristics including XMR suppression, superconducting transition, and discontinuous T_c evolution in a single material.

In this work, we confirm the link between XMR and superconductivity by studying LaBi, a recent topological semimetal that attracted attention due to its simple lattice and band structures.^{16–21} The three panels of Fig. 1 summarize our main findings: (a) The suppression of XMR by pressure is a purely electronic effect with no drastic changes in structural parameters, (b) Pressure suppresses XMR and induces superconductivity, and (c) The discontinuity in T_c at higher pressures is due to a structural transition.

II. METHODS

Single crystals of LaBi were grown using indium flux and characterized using powder x-ray diffraction and energy dispersive x-ray spectroscopy as explained in previous works.^{17,22} Low pressure measurements ($P < 2$ GPa) were performed in a piston-cylinder clamp cell using 40:60 mixture of light mineral oil:n-pentane as a hydrostatic medium. Pressure was measured from the superconducting transition of a Pb gauge placed beside the sample in the clamp cell.²³ The pressure cell was fit to a Quantum Design PPMS which monitored simultaneously the resistance of the sample, the Pb gauge, and a calibrated cernox sensor attached to the body of the cell for accurate thermometry. High pressure measurements were performed in a designer diamond anvil cell using steatite as the pressure transmitting medium and MP35N as the gasket material.²⁴ The designer diamond had eight tungsten micro-contacts centered on a 300 μm culet for electrical transport measurements. Pressure was measured by fluorescent spectroscopy on two pieces of ruby placed beside the sample in the diamond anvil cell.²⁵ A small single crystal of LaBi ($50 \times 50 \times 10 \mu\text{m}$) was placed inside the 120 μm diameter sample hole made by the electric discharge method. High pressure x-ray diffraction was performed in a membrane driven DAC with 300 μm culet diamond anvils and rhenium gasket with 120 μm hole filled with LaBi powder, copper powder as the pressure marker, and neon as the hydrostatic medium. Diffraction experiments took place at the Advanced Photon Source at Argonne National Laboratory (beamlines 16 ID-B and 13 ID-D) with 29.2 and 37.1 keV monochromatic x-ray beam. Angle dispersive diffraction patterns were collected with an area detector (Pilatus1M or Mar345) with exposure times ranging from 20-120 seconds. Two-dimensional x-ray diffraction images were in-

tegrated using FIT2D²⁶ software and refined using the EXPGUI/GSAS²⁷ software to extract structural parameters.

Band structure calculations are performed with the WIEN2k program using the general gradient approximation on augmented plane-waves and local orbitals.²⁸

III. RESULTS

Fig. 1 summarizes our main findings and provides a guide for the rest of the article. Fig. 1(a) shows the suppression of magnetoresistance $MR = 100 \times \frac{R(9T) - R(0)}{R(0T)}$ by pressure. Fig. 1(b) shows smooth compression of the cubic unit cell with no structural anomaly as the extreme magnetoresistance (XMR) is suppressed by pressure. Therefore, the suppression of XMR is due to smooth changes in the electronic structure of LaBi. At $P \approx 11$ GPa a discontinuity occurs in the unit cell volume due to a structural transition. Fig. 1(c) shows that bulk superconductivity ($R = 0$) starts at $P \approx 3.5$ GPa where XMR is substantially but not completely suppressed. The discontinuity in the pressure dependence of T_c at $P \approx 11$ GPa is due to the structural transition. In the rest of the paper, we elaborate the effect of pressure on magnetoresistance, crystal structure, and superconductivity in LaBi.

A. The effect of pressure on XMR

This section presents our data at lower pressures ($P < 3$ GPa), from clamp cell experiments, to focus on the suppression of XMR with pressure. Figs. 2(a-d) compare the normalized resistance $R(T)/R(300K)$, at $H = 0$ (blue) and $H = 9$ T (red), at $P = 0, 0.3, 1.6$, and 2.4 GPa. The red curve in Fig. 2(a) shows the typical profile of XMR with $\partial R/\partial T > 0$ at $T > 70$ K, $\partial R/\partial T < 0$ at $20 < T < 70$ K, and $\partial R/\partial T \rightarrow 0$ at $T < 20$ K. All topological semimetals with XMR show the same profile where $R(T)$ decreases initially with decreasing temperature, then increases, and finally saturates to a plateau.¹⁷ The blue curve at $H = 0$ shows metallic conduction where $R(T)$ decreases with decreasing temperature to a very small residual value. Such small residual resistance $R(0)$ is essential to having an extremely large ratio $R(H)/R(0)$ *i.e.* XMR.

Figs. 2(a-d) show a moderate increase of $R(H = 9$ T) in the plateau region ($T < 20$ K) from 0 to 0.34 GPa followed by a decrease at 1.6 GPa and a pronounced decrease at 2.4 GPa. These changes do not account for the systematic suppression of XMR as a function of pressure shown in Fig. 1(a). To understand the systematic decrease of XMR we turn attention to the zero field resistance $R(H = 0)$. Figs. 2(e-h) zoom into the normalized resistance at $H = 0$ and $T < 30$ K at $P = 0, 0.3, 1.6$, and 2.4 GPa to reveal a systematic increase of the zero-field resistance by increasing pressure. The black lines are fits

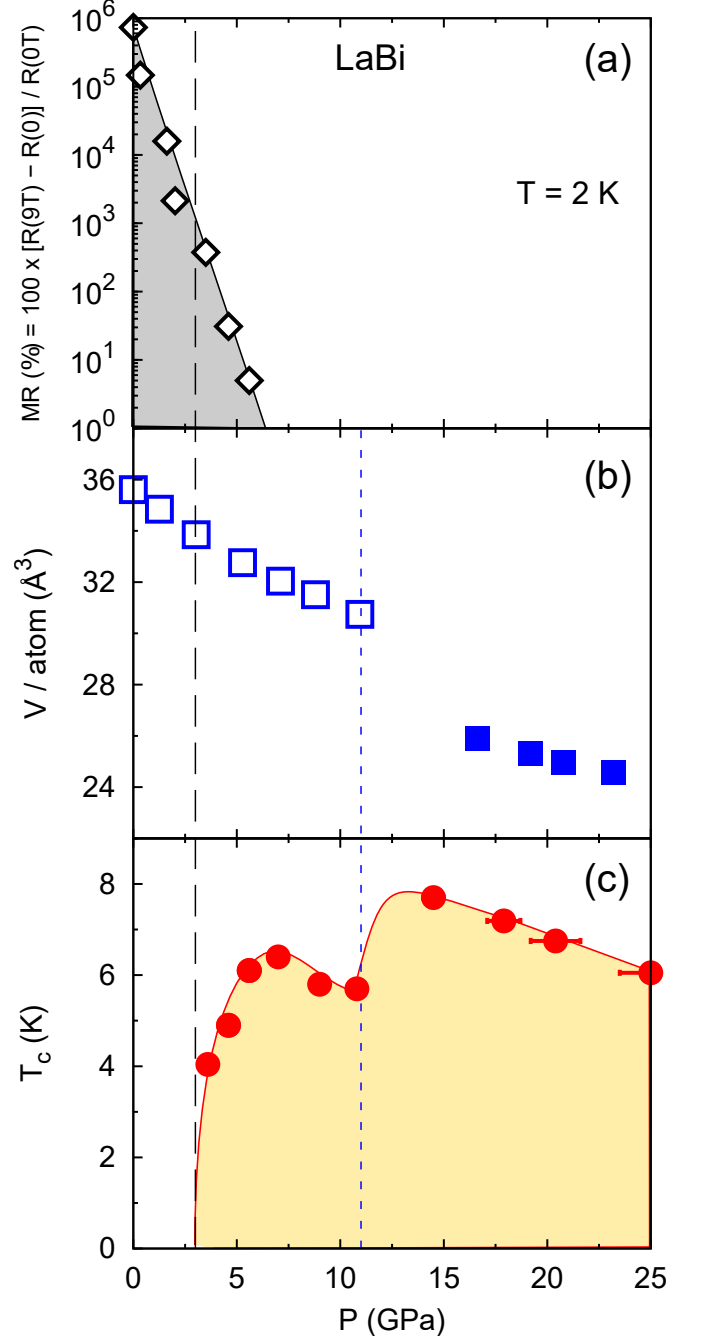


FIG. 1. (a) Magnetoresistance as a function of pressure in LaBi. The extreme magnetoresistance (XMR) is suppressed by $P \approx 5$ GPa. (b) Unit cell volume per atom as a function of pressure. Pressure reduces the cubic unit cell volume smoothly with no discontinuity across the region of XMR suppression. The discontinuous jump at $P \approx 11$ GPa is a structural transition from cubic to tetragonal marked by the vertical blue dotted line. (c) Temperature-pressure phase diagram of superconductivity in LaBi. The onset of superconductivity is marked by the vertical black dashed line. T_c increases rapidly with increasing pressure until $P = 6$ GPa, then decreases until $P = 11$ GPa where it shows a sudden 40% increase concurrent with the structural transition. For $P < 15$ GPa, errorbars are no larger than the size of the data points.

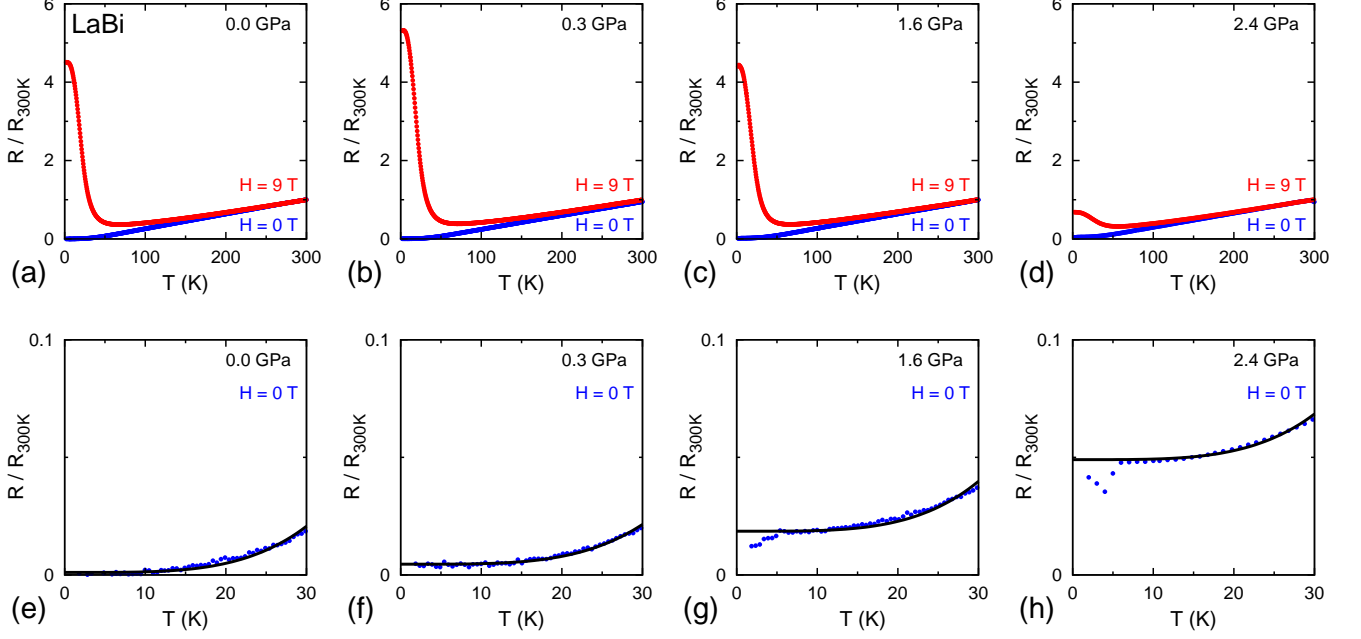


FIG. 2. Normalized resistance $R/R(300\text{K})$ at $H = 0$ (blue) and $H = 9$ T (red) as a function of temperature at $P = 0$ (a), $P = 0.3$ GPa (b), $P = 1.6$ GPa (c), and $P = 2.4$ GPa (d). The normalized resistance at $H = 9$ T in the plateau region is not systematically suppressed by increasing pressure and therefore does not explain the systematic suppression of XMR with pressure. A zoom into the normalized resistance $R/R(300\text{K})$ at $H = 0$ is shown for $T < 30$ K at $P = 0$ (e), $P = 0.3$ GPa (f), $P = 1.6$ GPa (g), and $P = 2.4$ GPa (h). Solid black lines are power law fits of the form $\rho = \rho_0 + AT^4$. The zero-field resistance systematically increases with increasing pressure which explains the systematic suppression of XMR. Broad and incomplete superconducting transitions appear at $P = 1.6$ and 2.4 GPa, most likely due to pressure inhomogeneity.

to the expression $\rho = \rho_0 + AT^4$ at each pressure. The systematic increase of the zero-field resistance in Fig. 2(e-h) explains the systematic decrease of XMR as a function of pressure in Fig. 1(a).

Fig. 3(a) visualizes the suppression of XMR with pressure by plotting $\text{MR} = 100 \times \frac{R(H) - R(0)}{R(0)}$ at $T = 2$ K as a function of field at $P = 0, 0.3, 1.6$, and 2.4 GPa. Fig. 3(b) highlights the systematic increase of $R(0)$ at $H = 0$ with increasing pressure. Fig. 3(c) shows a clear anti-correlation between increasing $R(0)$ and decreasing magnetoresistance. Both the left and the right y-axes are in logarithmic scale to compare the two quantities on equal footing. In contrast, Figs. 3(d) and 3(e) show the absence of a clear correlation between $R(9\text{ T})$ and XMR. Comparing Figs. 3(c) and 3(e) makes a compelling case that the zero-field resistance controls the magnitude of XMR in agreement with previous works that correlate the residual resistivity of various LaBi, LaSb, or WTe_2 samples with the magnitude of XMR.^{9,17,18} It has been proposed that a combination of orbital mixing, Fermi surface sizes, and Fermi surface shapes is responsible for the extremely small $R(0)$ in LaBi and other topological semimetals.^{17,19} Pressure is an effective tool to tune all of these parameters and therefore tuning the residual resistance of LaBi systematically as shown in Fig. 3(b).

B. The effect of pressure on the structure

Fig. 4(a) shows that the unit cell volume of LaBi smoothly decreases with increasing pressure until $P \approx 11$ GPa. There is no structural anomaly at lower pressures where extreme magnetoresistance is suppressed. At 11 GPa there is a discontinuous 10% drop in the unit cell volume due to a structural transition from the face centered cubic lattice (FCC, space group $Fm\bar{3}m$) to a primitive tetragonal lattice (PT, space group $P4/mmm$). The FCC to PT phase transition in LaBi has been theoretically predicted^{29–31} but experimentally unresolved until now. Fig. 4(a) shows that the onset of the structural transition at $P \approx 11$ GPa observed experimentally agrees with the theoretical predictions (thick green lines). Solid black lines in Fig. 4(a) are fits to the Birch-Murnaghan equation of state:^{32,33}

$$P(V) = \frac{3B}{2} \left[\left(\frac{V_0}{V} \right)^{\frac{7}{3}} - \left(\frac{V_0}{V} \right)^{\frac{5}{3}} \right] \times \left[1 + \frac{3}{4}(B' - 4) \left[\left(\frac{V_0}{V} \right)^{\frac{2}{3}} - 1 \right] \right] \quad (1)$$

where P_0 and V_0 are the coordinates of the first data points in the FCC and the PT phases. The bulk modulus B and its pressure derivative $B' = \partial B / \partial P$ in the low

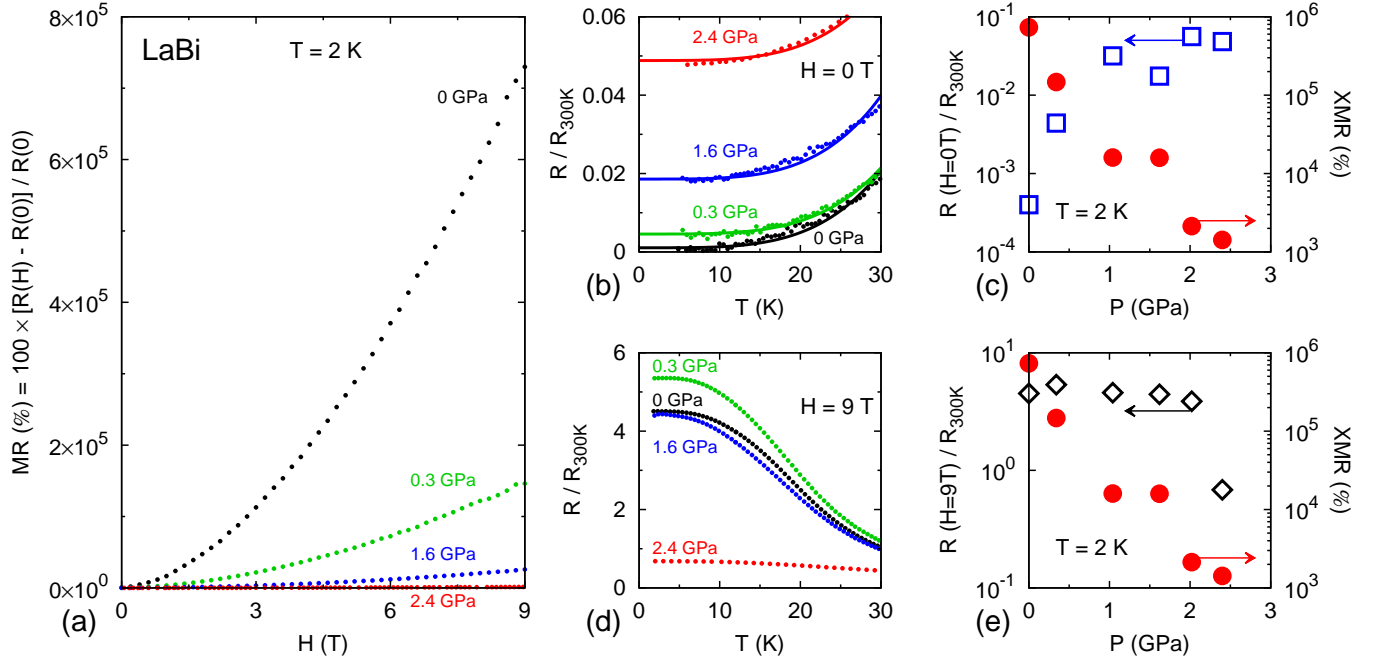


FIG. 3. (a) Magnetoresistance $MR = 100 \times \frac{R(H) - R(0)}{R(0)}$ at $T = 2$ K plotted as a function of field from $H = 0$ to 9 T at four representative pressure values. A systematic decrease of MR is observed with increasing pressure. (b) Normalized resistance $R/R(300\text{ K})$ as a function of temperature at $H = 0$ from $T = 5$ to 30 K. Solid lines are power law fits to the data at each pressure. A systematic increase of the normalized resistance is observed with increasing pressure. (c) Normalized resistance at $H = 0$ and $T = 2$ K are extracted from the fits in (b) and plotted as a function of pressure (empty blue squares corresponding to the left y-axis). XMR values at $H = 9$ T and $T = 2$ K are extracted from (a) and plotted as a function of pressure (red circles corresponding to the right y-axis). Both y-axes are logarithmic to show that the two quantities anti-correlate as they vary by orders of magnitude. (d) Normalized resistance $R/R(300\text{ K})$ as a function of temperature from $T = 2$ to 30 K at $H = 9$ T. (e) Normalized resistance at $H = 9$ T and $T = 2$ K are plotted as a function of pressure (empty black diamonds corresponding to the left y-axis). XMR values at $H = 9$ T and $T = 2$ K are extracted from (a) and plotted as a function of pressure (red circles corresponding to the right y-axis). There is no clear correlation between the two quantities.

pressure and the high pressure structures are extracted from the fits to Eq. 1 and summarized in table I. In the low pressure FCC structure, our experimental value for the bulk modulus agrees with the theoretical calculations by Cui *et al.*³¹ and Vaitheeswaran *et al.*²⁹. In the high pressure PT structure, the two theory groups disagree. Cui *et al.* predict comparable bulk moduli between the low and the high pressure structures. Vaitheeswaran *et al.* predict a two-fold increase of the bulk modulus in the high pressure PT structure. Our data clearly agrees with the latter (see table I). Representative powder x-ray diffraction data under pressure with Rietveld refinements are shown in Appendix A for both FCC and PT phases.

The structural transition at 11 GPa changes the band structure of LaBi as shown in Figs. 4(b) and 4(c). Fig. 4(b) shows the band structure of LaBi in the low pressure FCC structure with two hole-pockets at the Brillouin zone center Γ and one electron-pocket at X . The small circles represent lanthanum d -states and the large circles represent bismuth p -states. The mixing between d and p states on the electron pocket at X has been attributed to the extremely small $R(0)$ and the large $R(H)$ in LaBi.^{16,17} The combination of orbital mixing, small

ellipsoidal pockets, and electron-hole compensation as shown in Fig. 4(b) is common to all topological semimetals and possibly the source of XMR.¹⁷

Fig. 4(c) shows the electronic structure of LaBi in the high pressure PT phase with two notable changes compared to the low pressure FCC phase: (1) The hole-pocket near M is clearly larger than the electron-pocket near X and therefore electron-hole compensation is weaker in the PT phase. The lack of electron-hole compensation in the PT phase explains the lack of mag-

TABLE I. The bulk modulus B and its pressure derivative $B' = \partial B / \partial P$ for LaBi extracted by fitting the data to the Birch-Murnaghan equation of state (Eq. 1) as shown in Fig. 4(a). The initial parameters P_0 and V_0 were fixed based on the experimental data in the low pressure face centered cubic (FCC) and the high pressure primitive tetragonal (PT) structures.

Bravais Lattice	B (GPa)	B'	P_0 (GPa)	V_0 (\AA^3)
FCC	52 ± 1	5.0 ± 0.4	0	35.61
PT	97 ± 5	5.8 ± 0.9	16.6	25.90

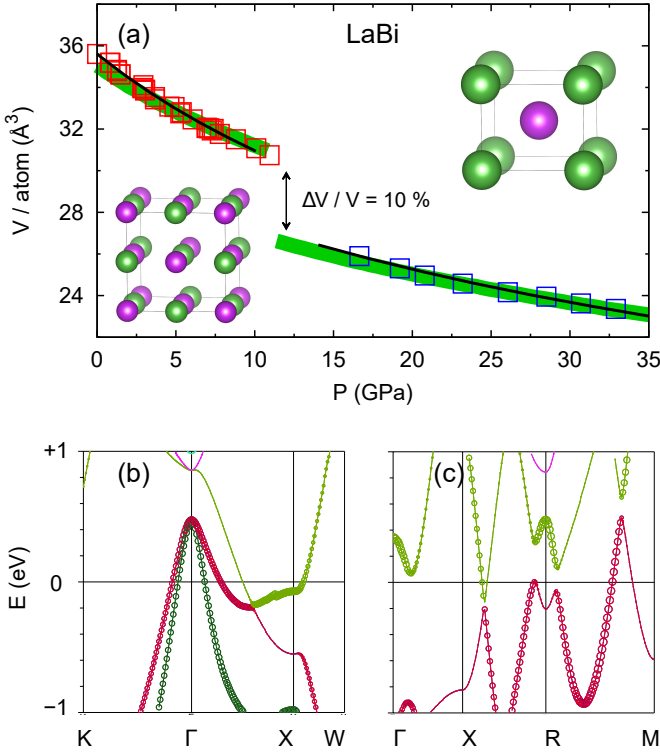


FIG. 4. (a) Unit cell volume per atom in LaBi as a function of pressure. The discontinuous drop at $P \approx 11$ GPa corresponds to a structural phase transition from face center cubic (FCC) to primitive tetragonal (PT) lattice as illustrated on the figure. Thick green lines are the results of theoretical calculations by Vaitheeswaran *et al.*²⁹ Solid black lines are fits to the Birch-Murnaghan equation of state (Eq. 1) from which we extract the bulk moduli for both structures as reported in table I. Representative refinements are given in Appendix A. (b) Band structure of LaBi in the low pressure FCC structure with two central hole-pockets at Γ and one electron-pocket at X. (c) Band structure of LaBi in the high pressure PT structure with a small electron-pocket at X, a larger hole-pocket at M, and a gap with band inversion at R.

netoresistance at high pressures. (2) There is a band inversion at the R point with a gap due to the spin-orbit coupling. Based on the Fu-Kane-Mele formula³⁴, this gap corresponds to a strong topological insulator. However, the hole-pocket that crosses E_F near M prevents LaBi from being an insulator. The detailed evolution of the band structure in LaBi under pressure is given in Appendix B.

C. The effect of pressure on superconductivity

Fig. 5(a) shows that the first complete superconducting transition ($R = 0$) appears at $P \approx 3.5$ GPa in LaBi. At this pressure, XMR is reduced by three orders of magnitude but not completely vanished as shown in Fig. 1(a). The onset of superconductivity is accompanied by two other observations, marked by the vertical black dashed

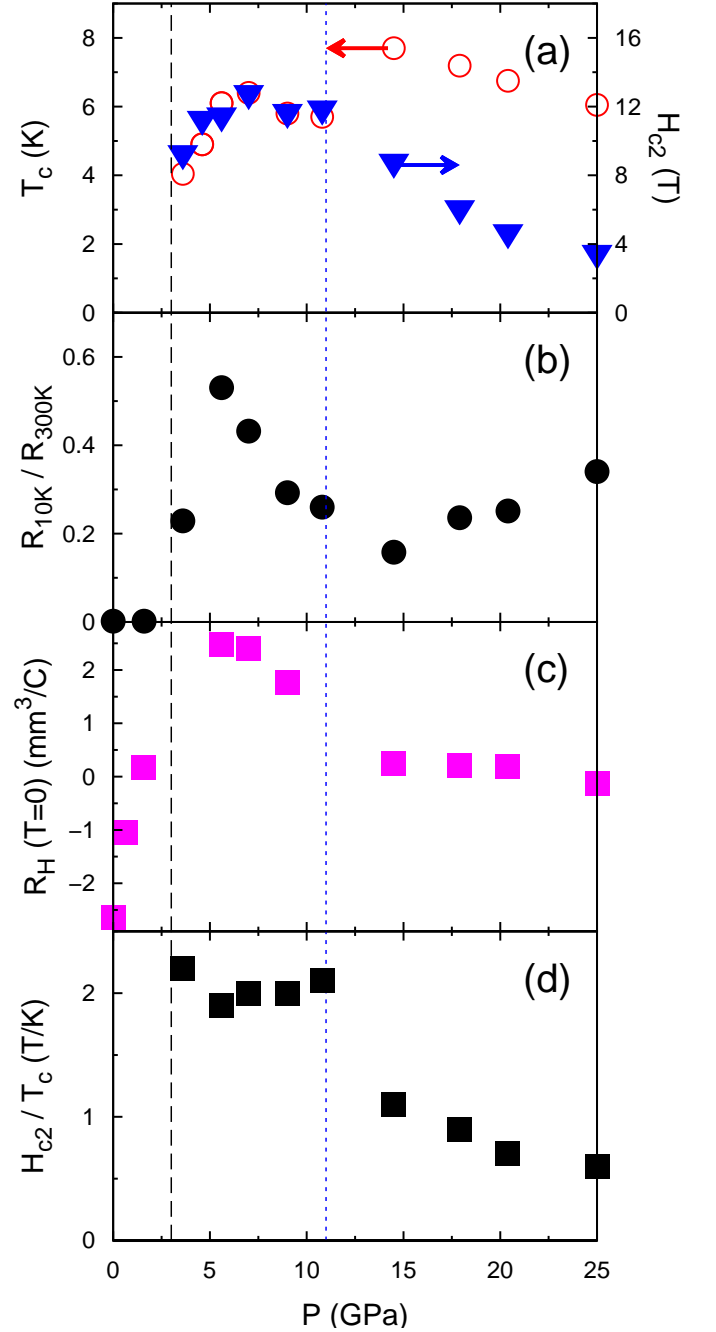


FIG. 5. (a) T_c and H_{c2} of LaBi as a function of pressure. Superconductivity onsets at $P \approx 3.5$ GPa, then T_c shows 40% enhancement at the structural transition at $P \approx 11$ GPa. (b) R_{10K}/R_{300K} plotted as a function of pressure in LaBi. The increase of R_{10K}/R_{300K} is associated with the suppression of XMR. At the structural transition ($P = 11$ GPa), R_{10K}/R_{300K} reverses direction from decreasing to increasing. (c) The zero temperature limit of the Hall coefficient R_H as a function of pressure. There is a sign change from negative to positive at low pressures in the region of XMR suppression just before superconductivity appears. R_H falls to almost zero at the structural transition at $P \approx 11$ GPa. (d) The ratio H_{c2}/T_c plotted as a function of pressure shows a sudden two-fold drop across the structural transition. The low pressure superconducting phase is not Pauli-limited but the high pressure phase is.

line on Fig. 5. First, the normalized low temperature resistance (R_{10K}/R_{300K}) shows considerable increase at the onset of superconductivity (also see Fig. 5(b)). Second, the Hall coefficient (R_H) changes sign (Fig. 5(c)). The complete temperature profiles of resistivity and Hall data are presented in Fig. 2 and Fig. 6. A change of sign in R_H concurrent with superconductivity was recently reported in another XMR material WTe_2 .¹¹ In Appendix B we use the experimental lattice parameters of LaBi to calculate the evolution of its band structure by increasing pressure. Fig. 9 in Appendix B shows that the electron pocket size reduces with pressure in agreement with the change of sign in R_H from negative to positive with increasing pressure as shown in Figs. 5(c) and 6(c). Ref. 17 argues that the electron pocket plays a central role in XMR which is consistent with our observation of simultaneous suppression of XMR, sign change in R_H , and the appearance of superconductivity.

The vertical blue dotted line on Fig. 5 marks the onset of structural transition at $P = 11$ GPa as discussed in section III B. Due to the structural transition, T_c shows a 40% increase (Fig. 5(a)), R_{10K}/R_{300K} reverses direction from decreasing to increasing (Fig. 5(b)), and R_H drops to almost zero (Fig. 5(c)). The complete $R(T)$ profiles are presented in Figs. 6(a) and 6(b). Such drastic changes in transport properties follow the drastic change of band structure as a result of the structural transition shown in Fig. 4.

Fig. 5(a) shows both T_c (left y-axis) and H_{c2} (right y-axis) at each pressure. The high values of H_{c2} and the onset of superconductivity at 3.5 GPa rule out Bismuth filamentary superconductivity which onsets at 8 GPa with $H_{c2} < 0.5$ T.^{35,36} Fig. 7 shows how we derive H_{c2} of LaBi using the extended Ginzburg-Landau formalism^{37,38}

$$H_{c2}(T) = H_{c2}(0) \frac{1 - (T/T_c)^2}{1 + (T/T_c)^2} \quad (2)$$

where $H_{c2}(0)$ is the upper critical field at $T = 0$. The values of $H_{c2} = 11.5$ T at $P = 5.6$ GPa and $H_{c2} = 6.1$ T at $P = 17.9$ GPa are order of magnitude larger than the reported values of H_{c2} in Bismuth.^{37,38} More details on Bi superconductivity are given in Appendix C.

Fig. 5(a) shows that before the structural transition at $P = 11$ GPa, H_{c2} values are almost double the value of T_c at each pressure. Since the Pauli limit of superconductivity is given by $H_{c2} = 1.85T_c$, the superconducting phase below 11 GPa seems not to be Pauli-limited. Interestingly, for $P > 11$ GPa *i.e.* after the structural transition, the ratio of H_{c2}/T_c suddenly drops to near unity. Fig. 5(d) traces the H_{c2}/T_c ratio as a function of pressure revealing the sudden transition from not-Pauli-limited superconductivity to Pauli-limited superconductivity across the structural transition. Spin triplet pairing is possible in the low pressure not-Pauli-limited phase but not in the high pressure Pauli-limited phase. Recent studies show a change of T_c with structural transition in $ZrTe_5$.¹³ It would be interesting to look for the same

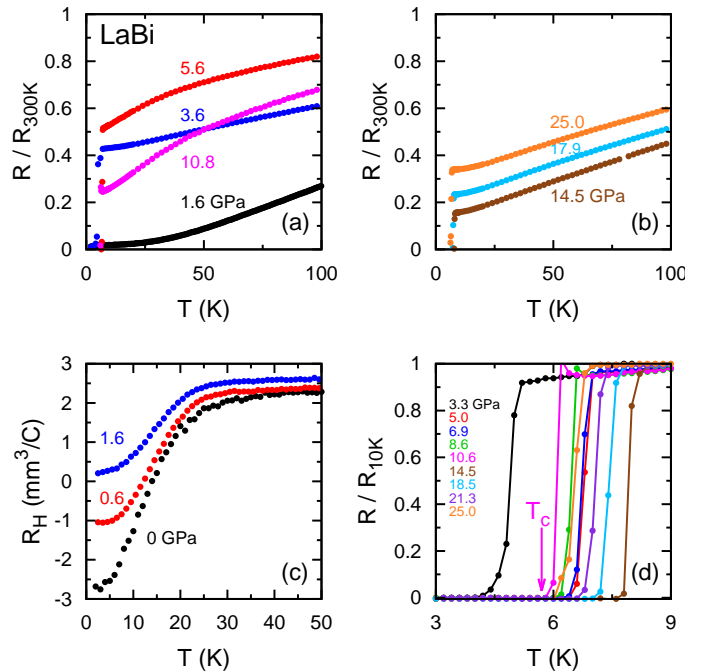


FIG. 6. (a) Normalized electrical resistance at $H = 0$ T, from $T = 2$ to 300 K, at several pressures below 11 GPa before the structural transition. (b) Normalized electrical resistance at $H = 0$ T, from $T = 2$ to 300 K, at several pressures above 11 GPa after the structural transition. (c) Hall coefficient as a function of temperature for several representative pressures. Note the sign change in $R_H(T = 0)$ with increasing pressure. (d) Normalized resistivity curves in the region of superconducting transition from which the phase diagrams in Figs. 1 and 5 are constructed. The arrow on the 10.6 GPa curve shows that we define T_c using $R = 0$ criterion.

effects in $ZrTe_5$ and other XMR materials which superconduct under pressure.

IV. SUMMARY

In summary, we study the effect of pressure on extreme magnetoresistance, crystal structure, and superconducting properties of LaBi. Pressure suppresses XMR and gives rise to superconductivity in LaBi (Fig. 1). The suppression of XMR anti-correlates with the increase of the residual resistance $R(0)$ as shown in Fig. 3(c). It does not correlate with the in-field resistance $R(9T)$ as shown in Fig. 3(e). The suppression of XMR is accompanied by a sign change in the Hall coefficient R_H from negative to positive as shown in Figs. 5(c) and 6(c). This is consistent with the recent argument that the electron Fermi surface with orbital mixing is responsible for the extremely small $R(0)$ and therefore XMR.¹⁷ Our DFT calculations in Fig. 9 in Appendix B confirm that the R_H sign change is due to the shrinking of the electron pocket with increasing pressure. The pressure induced structural transition in LaBi from FCC to PT shown in

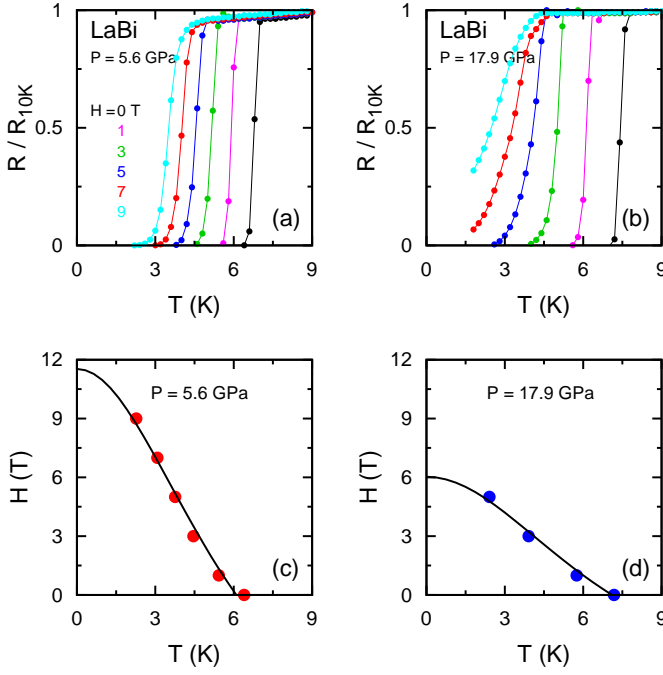


FIG. 7. (a) Normalized electrical resistance at $P = 5.6$ GPa plotted as a function of temperature in several magnetic fields as indicated on the figure. (b) Normalized electrical resistance at $P = 17.9$ GPa plotted as a function of temperature in several magnetic fields. (c) The H - T data for the superconducting transition from (a) are fitted to Eq. 2 with the resulting $H_{c2} = 11.5$ T. (d) The H - T data for the superconducting transition from (b) are fitted to Eq. 2 with the resulting $H_{c2} = 6.1$ T.

Fig. 4 is a new finding. The change in the crystal structure changes the band structure and creates a region of band inversion in LaBi (Fig. 4). The changes in the band structure of LaBi due to this structural transition give rise to a reversal in R_{10K}/R_{300K} from decreasing to increasing and a drop in R_H as shown in Figs. 5(b) and 5(c). At the structural transition, there is a discontinuity in T_c showing an abrupt 40% increase (Fig. 5(a)). Simultaneously, the ratio H_{c2}/T_c shows a step-like change from $H_{c2}/T_c \approx 2$ *i.e.* not-Pauli-limited superconductivity to $H_{c2}/T_c \approx 1$ *i.e.* Pauli-limited superconductivity as shown in Fig. 5(d).

ACKNOWLEDGMENTS

This work was performed under LDRD (Tracking Code No. 14-ERD-041) and under the auspices of the U.S. Department of Energy (DOE) by Lawrence Livermore National Laboratory (LLNL) under Contract No. DE-AC52-07NA27344. Portions of this work were performed at HPCAT (Sector 16), Advanced Photon Source (APS), Argonne National Laboratory. HPCAT operations are supported by the DOE-NNSA under Award No. DE-NA0001974 and the DOE-BES under Award No. DE-

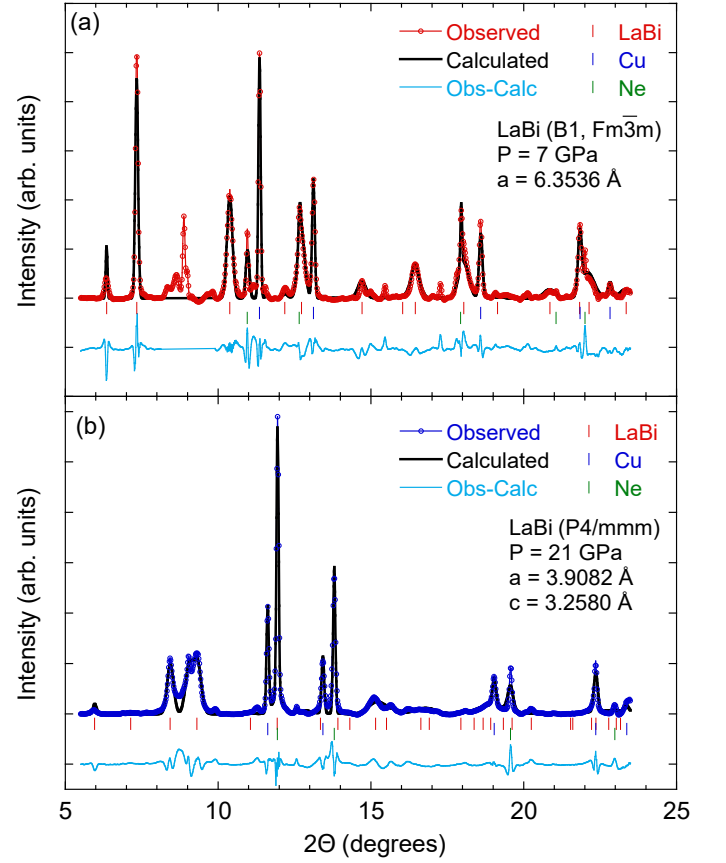


FIG. 8. Representative refinement of the x-ray diffraction patterns collected at (a) $P = 7$ GPa and (b) $P = 21$ GPa. Empty circles show the XRD data plotted as intensity versus 2θ . Black lines are the best fit to the data. Blue lines show the difference between the data and the fits. Cu (pressure gauge) and Ne (pressure transmitting medium) peaks are indexed individually.

FG02-99ER45775 with partial instrumentation funding by the NSF. The Advanced Photon Source is a U.S. DOE Office of Science User Facility operated for the DOE Office of Science by Argonne National Laboratory under Contract No. DE-AC02-06CH11357. Beam time was provided by the Carnegie DOE-Alliance Center (CDAC). Y.K.V. acknowledges support from DOE-NNSA Grant No. DE-NA0002014. The research at Princeton was supported by the Gordon and Betty Moore Foundation under the EPiQS program, grant GBMF 4412 and the ARO MURI on topological insulators, grant W911NF-12-1-0461.

Appendix A: Rietveld refinement of high pressure XRD data

Fig. 8 includes two representative structural refinements of the x-ray diffraction data at $P = 7$ GPa and $P = 21$ GPa. The low pressure structure is rock-salt (B1) and the high pressure structure has a primitive tetrago-

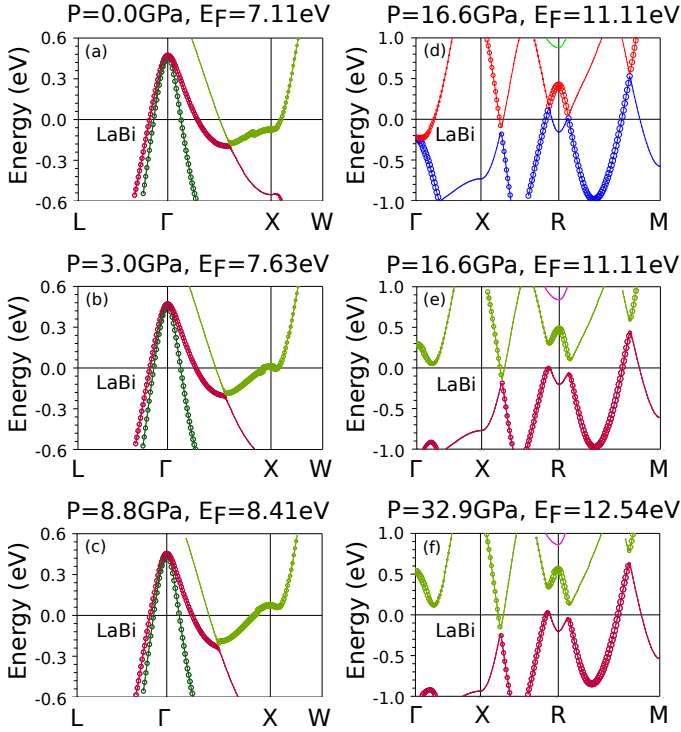


FIG. 9. (a) Band structure of LaBi at $p = 0$ in the FCC structure. The large circles represent the p -orbitals of Bi and the small circles represent the d -orbitals of La. The y-axis is energy relative to E_F with the E_F given on top of each panel. (b) Band structure of LaBi at $p = 3.0$ GPa. Notice that the electron pocket shrinks in size and its shape changes from cylindrical to round. (c) Band structure of LaBi at $p = 8.8$ GPa. The electron pocket continues to shrink and become more spherical. Notice that the Fermi energy E_F increases with increasing pressure and makes the material less compensated. (d) Band structure of LaBi at $p = 16.6$ GPa in the PT structure after the structural transition. This calculation is without spin-orbit coupling to show the mixing between the bands at R . (e) After including SOC, the bands hybridize and a gap opens at R with a clear band inversion. (f) Band structure of LaBi at $p = 32.9$ GPa in the PT structure. Pressure does not change the band structure that much in this phase.

nal unit cell as illustrated on Fig. 4. In Fig. 8(a), the peaks between 8 and 9 degrees have been excluded from the refinement, and they are likely to come from small inclusions of elemental Bi. At 7 GPa, Bi is in a complex host-guest structure, which is difficult to refine with so few evident peaks. For $P > 8$ GPa, elemental Bi is BCC, and we do include this phase in the refinement; the most prominent Bi peak occurs near 9 degrees in Fig 7b.

Appendix B: Evolution of LaBi band structure with pressure

Figs. 9(a-c) present the band structure of LaBi in the FCC structure at $P = 0, 3.0$, and 8.8 GPa before the structural transition. Larger circles represent Bi p -states

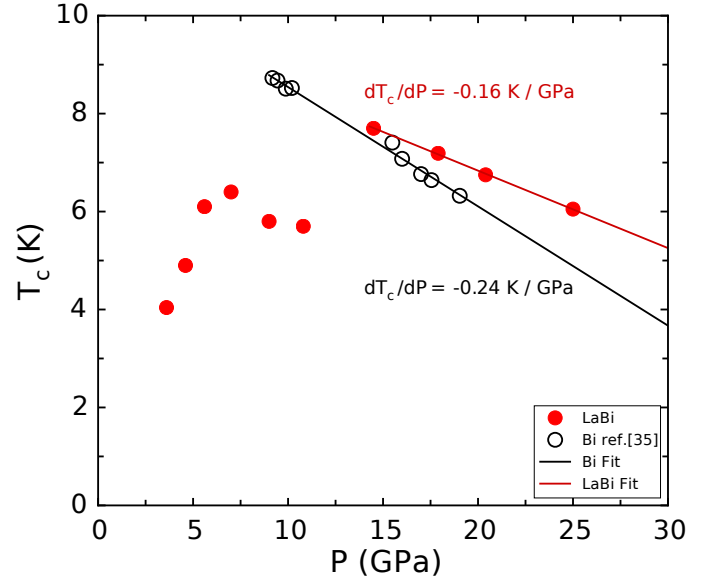


FIG. 10. T_c plotted as a function of pressure in LaBi (solid red circles) and Bi (open black circles). Data points for Bi come from Ref. 35. Superconductivity in Bi starts from $P = 8$ GPa with higher T_c than LaBi at the same pressure. We do not see short circuiting due to Bi superconductivity. Also note that the pressure slope of T_c in Bi is 1.5 times larger than LaBi.

and smaller circles represent La d -states. The calculation is based on our experimental values for the lattice parameters of LaBi (see Fig. 4). With increasing pressure, the Fermi energy E_F increases and the size of the electron pocket at X shrinks. Pressure also changes the shape of this pocket from cigar-shape to round. Figs. 9(d-f) present the band structure in the PT structure after the structural transition at $P = 16.6$ and 32.9 GPa. Fig. 9(d) shows the results of DFT calculations in the PT structure before including spin-orbit coupling. As a result of SOC, the two bands that cross at R will hybridize to form a band inverted gap as shown in Fig. 9(e). Increasing pressure in the PT phase does not change the band structure visibly as shown in Fig. 9(f) which is due to the stiffer structure in the PT phase (table I). The band structure plotted in Fig. 9(a) gives rise to the extreme magnetoresistance and a negative R_H in LaBi, in (b) XMR is reduced, R_H has changed sign to positive, and the material is on the verge of becoming a superconductor, in (c) XMR is completely gone and the material is superconducting in the FCC structure with $H_{c2}/T_c \approx 2$, in (e) the material has gone through the structural phase transition, it continues to superconduct in the PT structure but with $H_{c2}/T_c \approx 1$, in (f) LaBi is still superconducting in the PT phase with R_H becoming nearly zero.

Appendix C: Superconductivity in LaBi and Bi

In the main text we mentioned two reasons to believe that the superconducting transitions we observe do not come from elemental Bismuth: (a) Superconductivity of Bi starts at lower pressures with higher T_c , and (b) it has a much lower H_{c2} .^{35,36} Fig. 10 shows the pressure dependence of T_c in Bi from Ref. 35 in open black symbols and compares it to our data in LaBi as full red symbols. Superconductivity in Bi onsets at $P = 8$ GPa with $T_c = 8.9$ K. At the same pressure, $T_c = 5.8$ K in LaBi. If the superconducting signal was due to elemental Bi, it should

have short circuited the resistivity of LaBi and mask the transition at 5.8 K. Further, the pressure dependence of T_c in LaBi at high pressures has a slope $dT_c/dP = -0.16$ K/GPa compared to Bi with $dT_c/dP = -0.24$ which is 1.5 times larger. Lastly, the H_{c2} values we extract for LaBi as shown in Fig. 7 are a few teslas compared to H_{c2} , 0.5 T in elemental Bismuth.^{35,36} Therefore, the superconducting transitions observed here cannot come from Bi impurity phases. LaBi is grown out of Indium flux which also superconducts with $T_c = 3.4$ K at zero pressure. We clearly do not see any superconducting transitions at zero pressure and the first complete transition appears at 3.5 GPa which cannot be due to indium because the T_c of indium decreases with pressure.

-
- * fazel.tafti@bc.edu
- ¹ T. Liang, Q. Gibson, M. N. Ali, M. Liu, R. J. Cava, and N. P. Ong, *Nature Materials* **14**, 280 (2015).
 - ² J. Xiong, S. K. Kushwaha, T. Liang, J. W. Krizan, M. Hirschberger, W. Wang, R. J. Cava, and N. P. Ong, *Science* **350**, 413 (2015).
 - ³ C. Shekhar, A. K. Nayak, Y. Sun, M. Schmidt, M. Nicklas, I. Leermakers, U. Zeitler, Y. Skourski, J. Wosnitza, Z. Liu, Y. Chen, W. Schnelle, H. Borrmann, Y. Grin, C. Felser, and B. Yan, *Nature Physics* **11**, 645 (2015).
 - ⁴ N. J. Ghimire, Y. Luo, M. Neupane, D. J. Williams, E. D. Bauer, and F. Ronning, *Journal of Physics: Condensed Matter* **27**, 152201 (2015).
 - ⁵ X. Huang, L. Zhao, Y. Long, P. Wang, D. Chen, Z. Yang, H. Liang, M. Xue, H. Weng, Z. Fang, X. Dai, and G. Chen, *Physical Review X* **5**, 031023 (2015).
 - ⁶ K. Wang, D. Graf, L. Li, L. Wang, and C. Petrovic, *Scientific Reports* **4** (2014).
 - ⁷ Z. Wang, Y. Li, Y. Lu, Z. Shen, F. Sheng, C. Feng, Y. Zheng, and Z. Xu, arXiv:1603.01717 [cond-mat] (2016), arXiv: 1603.01717.
 - ⁸ M. N. Ali, J. Xiong, S. Flynn, J. Tao, Q. D. Gibson, L. M. Schoop, T. Liang, N. Haldolaarachchige, M. Hirschberger, N. P. Ong, and R. J. Cava, *Nature* **514**, 205 (2014).
 - ⁹ M. N. Ali, L. Schoop, J. Xiong, S. Flynn, Q. Gibson, M. Hirschberger, N. P. Ong, and R. J. Cava, *EPL (Europhysics Letters)* **110**, 67002 (2015).
 - ¹⁰ T. M. Tritt, N. D. Lowhorn, R. T. Littleton, A. Pope, C. R. Feger, and J. W. Kolis, *Physical Review B* **60**, 7816 (1999).
 - ¹¹ D. Kang, Y. Zhou, W. Yi, C. Yang, J. Guo, Y. Shi, S. Zhang, Z. Wang, C. Zhang, S. Jiang, A. Li, K. Yang, Q. Wu, G. Zhang, L. Sun, and Z. Zhao, *Nature Communications* **6**, 7804 (2015).
 - ¹² X.-C. Pan, X. Chen, H. Liu, Y. Feng, Z. Wei, Y. Zhou, Z. Chi, L. Pi, F. Yen, F. Song, X. Wan, Z. Yang, B. Wang, G. Wang, and Y. Zhang, *Nature Communications* **6**, 7805 (2015).
 - ¹³ Y. Zhou, J. Wu, W. Ning, N. Li, Y. Du, X. Chen, R. Zhang, Z. Chi, X. Wang, X. Zhu, P. Lu, C. Ji, X. Wan, Z. Yang, J. Sun, W. Yang, M. Tian, Y. Zhang, and H.-k. Mao, *Proceedings of the National Academy of Sciences* **113**, 2904 (2016).
 - ¹⁴ Y. Qi, W. Shi, P. G. Naumov, N. Kumar, W. Schnelle, O. Barkalov, C. Shekhar, H. Borrmann, C. Felser, B. Yan, and S. A. Medvedev, arXiv:1602.08616 [cond-mat] (2016), arXiv: 1602.08616.
 - ¹⁵ Y. Qi, P. G. Naumov, M. N. Ali, C. R. Rajamathi, W. Schnelle, O. Barkalov, M. Hanfland, S.-C. Wu, C. Shekhar, Y. Sun, V. S. M. Schmidt, U. Schwarz, E. Pippel, P. Werner, R. Hillebrand, T. Frster, E. Kampert, S. Parkin, R. J. Cava, C. Felser, B. Yan, and S. A. Medvedev, *Nature Communications* **7**, 11038 (2016).
 - ¹⁶ M. Zeng, C. Fang, G. Chang, Y.-A. Chen, T. Hsieh, A. Bansil, H. Lin, and L. Fu, arXiv:1504.03492 [cond-mat] (2015), arXiv: 1504.03492.
 - ¹⁷ F. F. Tafti, Q. Gibson, S. Kushwaha, J. W. Krizan, N. Haldolaarachchige, and R. J. Cava, *Proceedings of the National Academy of Sciences* **113**, E3475 (2016).
 - ¹⁸ F. F. Tafti, Q. D. Gibson, S. K. Kushwaha, N. Haldolaarachchige, and R. J. Cava, *Nature Physics* **12**, 272 (2016).
 - ¹⁹ L.-K. Zeng, R. Lou, D.-S. Wu, P.-J. Guo, L.-Y. Kong, Y.-G. Zhong, J.-Z. Ma, B.-B. Fu, P. Richard, P. Wang, G. T. Liu, L. Lu, S.-S. Sun, Q. Wang, L. Wang, Y.-G. Shi, H.-C. Lei, K. Liu, S.-C. Wang, T. Qian, J.-L. Luo, and H. Ding, arXiv:1604.08142 [cond-mat] (2016), arXiv: 1604.08142.
 - ²⁰ Y. Wu, T. Kong, L.-L. Wang, D. D. Johnson, D. Mou, L. Huang, B. Schrunck, S. L. Bud'ko, P. C. Canfield, and A. Kaminski, arXiv:1604.08945 [cond-mat] (2016), arXiv: 1604.08945.
 - ²¹ J. Nayak, S.-C. Wu, N. Kumar, C. Shekhar, S. Singh, J. Fink, E. E. D. Rienks, G. H. Fecher, S. S. P. Parkin, B. Yan, and C. Felser, arXiv:1605.06997 [cond-mat] (2016), arXiv: 1605.06997.
 - ²² S. Sun, Q. Wang, P.-J. Guo, K. Liu, and H. Lei, arXiv:1601.04618 [cond-mat] (2016), arXiv: 1601.04618.
 - ²³ A. Eiling and J. S. Schilling, *Journal of Physics F: Metal Physics* **11**, 623 (1981).
 - ²⁴ S. T. Weir, J. Akella, C. Aracne-Ruddle, Y. K. Vohra, and S. A. Catledge, *Applied Physics Letters* **77**, 3400 (2000).
 - ²⁵ G. J. Piermarini, S. Block, J. D. Barnett, and R. A. Forman, *Journal of Applied Physics* **46**, 2774 (1975).
 - ²⁶ A. P. Hammersley, S. O. Svensson, M. Hanfland, A. N. Fitch, and D. Hausermann, *High Pressure Research* **14**, 235 (1996).

- ²⁷ B. H. Toby, *Journal of Applied Crystallography* **34**, 210 (2001).
- ²⁸ P. Blaha, K. Schwarz, G. Madsen, D. Kvasnicka, and J. Luitz, *WIEN2K, An Augmented Plane Wave + Local Orbitals Program for Calculating Crystal Properties* (Karlheinz Schwarz, Techn. Universitt Wien, Austria, Wien, Austria, 2001).
- ²⁹ G. Vaitheeswaran, V. Kanchana, and M. Rajagopalan, *Physica B: Condensed Matter* **315**, 64 (2002).
- ³⁰ Z. Charifi, A. H. Reshak, and H. Baaziz, *Solid State Communications* **148**, 139 (2008).
- ³¹ S. Cui, W. Feng, H. Hu, Z. Feng, and H. Liu, *Solid State Communications* **149**, 996 (2009).
- ³² F. D. Murnaghan, *American Journal of Mathematics* **59**, 235 (1937).
- ³³ F. Birch, *Physical Review* **71**, 809 (1947).
- ³⁴ L. Fu, C. L. Kane, and E. J. Mele, *Physical Review Letters* **98**, 106803 (2007).
- ³⁵ M. Il'ina, E. Itskevich, and E. Dizhur, *Low Temperature Physics* **34**, 1263 (1972).
- ³⁶ L. A. Baring, R. R. d. Silva, and Y. Kopelevich, *Low Temperature Physics* **37**, 889 (2011).
- ³⁷ X. Zhu, H. Yang, L. Fang, G. Mu, and H.-H. Wen, *Superconductor Science and Technology* **21**, 105001 (2008).
- ³⁸ L. Fang, Y. Wang, P. Y. Zou, L. Tang, Z. Xu, H. Chen, C. Dong, L. Shan, and H. H. Wen, *Physical Review B* **72**, 014534 (2005).